Ore Geology Reviews 90 (2017) 25–35

Contents lists available at ScienceDirect

Ore Geology Reviews

journal homepage: www.elsevier.com/locate/oregeorev

Quartz chemistry – A step to understanding magmatic-hydrothermal processes in ore-bearing granites: Cínovec/Zinnwald Sn-W-Li deposit, Central Europe

Karel Breiter[a,*], Jana Ďurišová[a], Marek Dosbaba[b]

[a] Institute of Geology of the Czech Academy of Sciences, Rozvojová 269, CZ-16500 Praha 5, Czech Republic
[b] Tescan Company, Libušina třída 21, CZ-623 00 Brno, Czech Republic

ARTICLE INFO

Keywords:
Quartz
Trace elements
Cínovec
Zinnwald
Erzgebirge
LA-ICP-MS

ABSTRACT

Quartz from granites, greisens and quartz veins from a 1596 m long vertical section through the Cínovec/Zinnwald Li-Sn-W deposit (Czech Republic) was studied using cathodoluminescence (CL) and laser ablation inductively coupled plasma mass spectrometry (LA-ICP MS). The trace contents of Al, Ti, Li and the Ge/Ti and Al/Ti values in quartz reflect the degree of fractionation of parental melt from which primary quartz crystallized. From the biotite granite to the younger zinnwaldite granite, quartz is characterized by increasing contents of Al (from 136–176 to 240–280 ppm) and decreasing Ti (from 16–54 to 6–14 ppm), while the contents of Li and Ge are similar (15–36 and 0.8–1.7 ppm, respectively). Quartz of the greisen stage and vein stage is poor in all measured elements (26–59 ppm Al, 0.5–1.6 ppm Ti, 2–13 ppm Li, 0.8–1.6 ppm Ge). The youngest low-temperature quartz forming thin coatings in vugs in greisen and veins differs in its extreme enrichment in Al (> 1000 ppm) and Li (~100 ppm) and very low Ti (< 1 ppm). Within the greisen, remnants of primary magmatic quartz should be distinguished from metasomatic greisen-stage quartz in their higher intensity of CL and relatively higher Ti contents. A part of primary magmatic quartz may by secondarily purified *via* infiltration of hydrothermal fluids and dissolution–reprecipitation processes. Such quartz parallels newly formed greisen-stage quartz in its chemical and CL properties; the share of greisen-stage quartz may by therefore overestimated.

1. Introduction

The study of trace-element chemical composition of quartz can be still considered an emerging geological discipline, due to analytical challenges caused by low trace element contents. Attempts to analyze dissolute quartz (Monecke et al., 2002; Götze et al., 2004) are questioned because of a practical impossibility to achieve really monomineralic quartz concentrate without microscopic mineral and fluid inclusions. After a short episode of application of electron microprobe analyses (EMPA, Müller et al., 2003; Larsen et al., 2009; Donovan et al., 2011), the laser ablation inductively coupled plasma mass spectrometry (LA-ICP MS, Flem et al., 2002) has become the standard method for *in situ* quartz microanalyses. Along with the study of chemical composition, the internal fabric of quartz is commonly studied by cathodoluminescence (CL, D'Lemos et al., 1997; Müller et al., 2000; Rusk et al., 2008; Götte et al., 2011; Frelinger et al., 2015).

During the last 15 years, several tens of studies provided a good overview of trace element contents in quartz from granites (Müller et al., 2008b, 2010; Breiter and Müller, 2009; Larsen et al., 2009; Jacamon and Larsen, 2009; Breiter et al., 2013), pegmatites (Larsen et al., 2004; Müller et al., 2008a; Beurlen et al., 2011; Breiter et al., 2014; Garate-Olave et al., 2017), rhyolites (Müller et al., 2010; Breiter et al., 2012), and sulfide-bearing hydrothermal deposits (Rusk et al., 2006, 2008; Takahashi et al., 2007; Götte et al., 2011). Relatively scarce data have been published from metamorphic rocks (Monecke et al., 2002; Müller and Koch-Müller, 2009) and, surprisingly, little attention has been given to high-temperature greisen-style deposit (Breiter et al., 2017a).

We decided to utilize the extensive study material from the well-known greisen-type Sn-W-Li deposit of Cínovec/Zinnwald in the Erzgebirge including a 1.6 km deep borehole CS-1 to perform a detailed study of Cínovec quartz with two main objectives: (i) to decipher the vertical zoning of quartz composition through an ore-bearing granite pluton, and (ii) to define differences in the composition between magmatic and hydrothermal (greisen-stage) quartz.

* Corresponding author.
E-mail address: breiter@gli.cas.cz (K. Breiter).

http://dx.doi.org/10.1016/j.oregeorev.2017.10.013
Received 27 July 2017; Received in revised form 10 October 2017; Accepted 15 October 2017
Available online 16 October 2017
0169-1368/ © 2017 Elsevier B.V. All rights reserved.

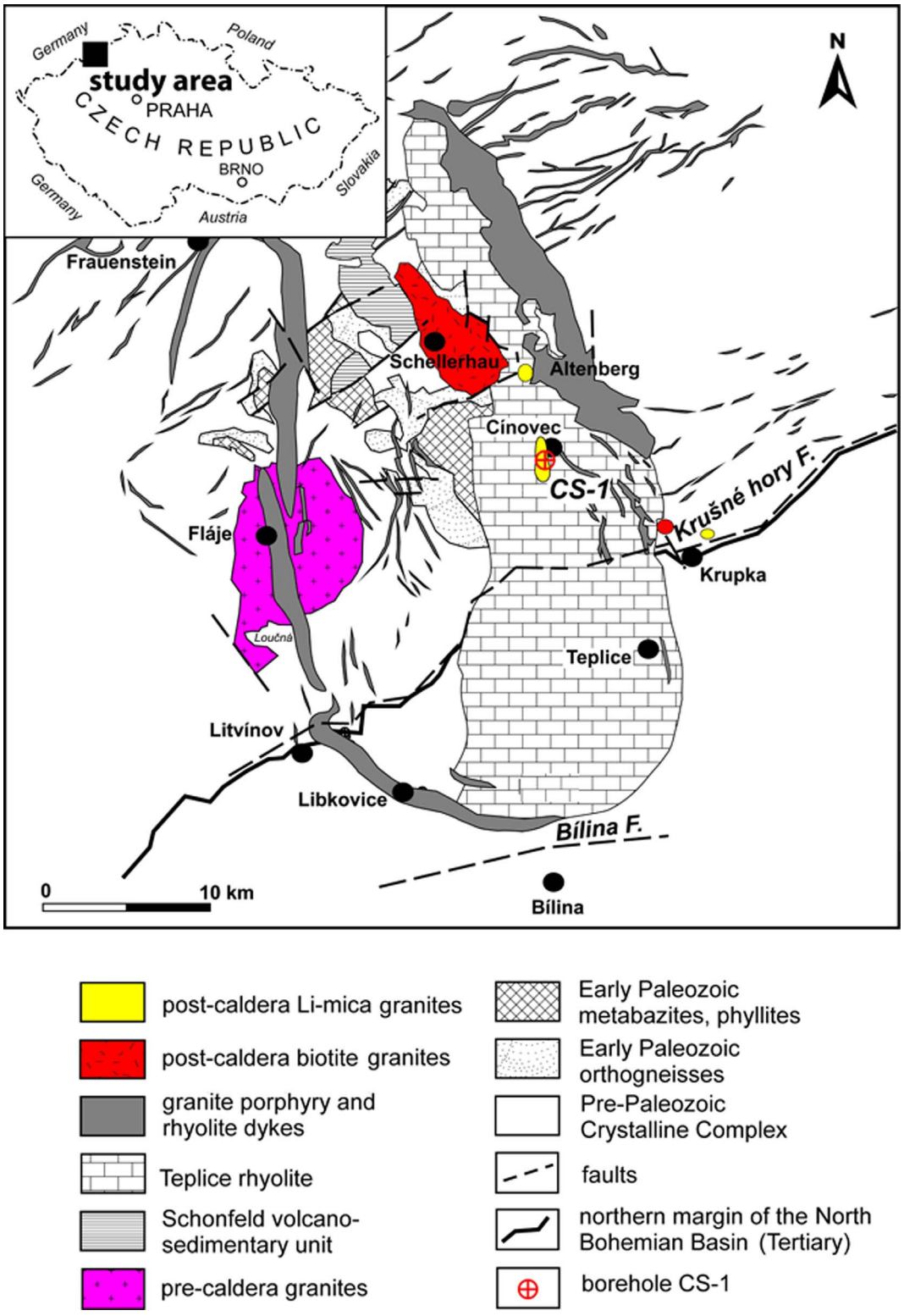

Fig. 1. Geological sketch of the Altenberg–Teplice caldera.

2. Geology and samples

The Cínovec granite cupola lies on both sides of the Czech–German border in the eastern sector of the Krušné Hory/Erzgebirge Mts. The dominant geological structure of the Eastern Krušné Hory is the Altenberg–Teplice caldera (Walther et al., 2016), approximately 40 × 20 km in size (Fig. 1). A detailed knowledge of its stratigraphy (Breiter, 1997) permits to establish the sequence of Variscan magmatic events:

- intrusion of barren peraluminous biotite granites (e.g. Fláje pluton),
- eruption of peraluminous rhyolite–dacite lava and tuffs (Schönfeld Volcanosedimentary Unit),
- rhyolite volcanism of A-type ("Teplice rhyolite") in three stages,
- collapse of the rhyolite volcano and creation of the Altenberg–Teplice caldera, intrusion of ring dykes of granite

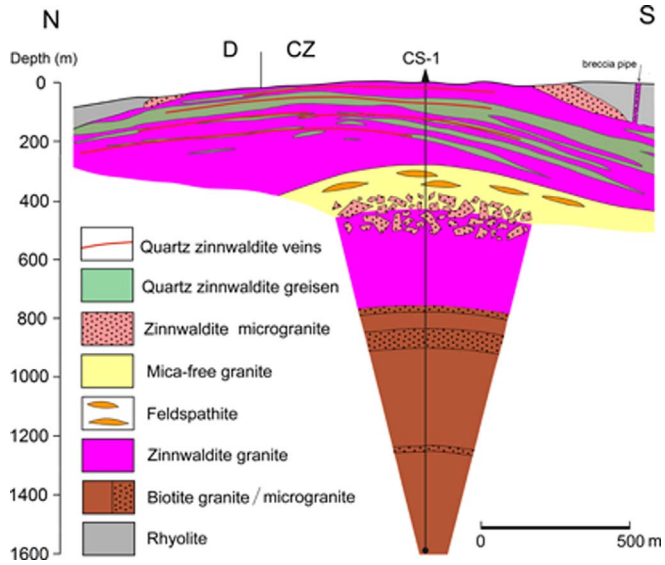

Fig. 2. Geological section through the Cínovec granite pluton.

porphyry,

- intrusion of biotite granite of A-type without ore-bearing hydrothermal activity at Preiselberg and Schellerhau,
- intrusion of strongly fractionated ore-bearing Li-mica rare-metal granite (RMG) of A-type.

The A-type granites formed a mostly hidden subsurface ridge intersecting the caldera from NW to SE with several local elevations. The two largest are the Cínovec/Zinnwald (Czech and German synonyms) and the Altenberg cupolas, rising to the present surface. A specific feature of the RMGs in the Erzgebirge is their intrusion into the subvolcanic level, as proved by the formation of explosive breccia pipes (Seltmann et al., 1987).

The Cínovec granite cupola exposure 1.4 × 0.3 km in size was studied to a depth of 1596 m by borehole CS-1 (Štemprok and Šulcek, 1969; Breiter et al., 2017b). An albite-topaz-zinnwaldite granite (referred to as "zinnwaldite granite", ZiG) was proved to be present in several textural varieties to a depth of 735 m, while an albite-biotite granite (referred to as "biotite granite", BtG) continues to greater depths (Fig. 2). Fractionation *in situ* can be observed in zinnwaldite granite, showing upward increasing concentrations of volatile and lithophile elements. The apical part of the cupola has been eroded, but a facies with mica corresponding to lepidolite is preserved to a depth of ca. 80 m below the present surface (Rub et al., 1998). Specific facies of ZiG represents the fine-grained rapidly cooled matrix of an explosive breccia in the hanging wall of the cupola (Fig. 2). From the viewpoint of geochemistry, the Cínovec pluton represents strongly fractionated A-type granites: it is only slightly peraluminous, enriched in F, Li, Rb, Zr, Th, HREE, Sc, Sn, W, Nb and Ta, and depleted in P, Ti, Mg and Ca (Breiter et al., 2017b). Common accessory minerals comprise fluorite, topaz, cassiterite, columbite, microlite, pyrochlore, Nb-rutile, zircon, thorite, xenotime, fluorides, oxo-fluorides and carbonates of REE (Cocherie et al., 1991; Johan and Johan, 1994; Rub et al., 1998; Breiter et al., 1999; Förster et al., 1999; Breiter and Škoda, 2012, 2017).

Brief data on the chemical composition of granitic quartz from Cínovec were published within regional studies about the Altenberg–Teplice caldera (Breiter et al., 2012) and a comprehensive study about granites from the Bohemian Massif (Breiter et al., 2013). The data set was now complemented with a detailed study of quartz from greisen, quartz veins and matrix of an explosive breccia (Table 1).

3. Methods

3.1. Cathodoluminescence (CL)

The panchromatic CL images of whole thin sections were obtained using a TESCAN MIRA3 scanning electron microscope with a field emission electron source. The images were obtained using a single-channel Panchromatic CL detector equipped with a quartz glass light guide transparent in the range of 185–850 nm. A working distance of 15 mm was used for all samples. The accelerating voltage and current were set to 25 kV and 15 nA, respectively. The scanning speed ranged from 100 to 1000 µs/pixel depending on the CL emissivity of the imaged area.

3.2. Trace elements analyses of quartz

The contents of trace elements Al, B, Be, Fe, Ge, Li, Mn, P, Rb, Sn, Sr, and Ti in quartz were determined using laser ablation inductively coupled plasma mass spectrometry (LA-ICP-MS) at the Institute of Geology CAS. This involved a Thermo-Finnigan Element 2 sector field mass spectrometer coupled with an Analyte Excite 193 nm excimer Laser (Photon Machines). Laser was fired at a repetition rate of 10 Hz, laser fluence of 4–5 J/cm^2 and beam size of 100 µm. The ablated material was transported by a high-purity He gas from the laser ablation cell. Time-resolved signal data were processed using the Glitter software (http://www.glitter-gemoc.com/). The isotope ^{29}Si was used as the internal standard based on the assumption that the analyzed quartz contains 99.95 wt% SiO_2. Data were calibrated against the external standard of synthetic silicate glass NIST SRM 612. For more details, see Breiter et al. (2012). Because a well characterized matrix-matched quartz reference material is missing, it is not possible to quantify the analytical accuracy. In order to monitor the reproducibility of the standardization method, we analyzed NIST SRM 1830 as an unknown along with each set of quartz samples. The relative deviation between the measured and reference concentrations (Flem and Bédard, 2002) were better than 10% for all elements except Al and Ge, which were underestimated by 20% and 16%, respectively. Up to 20% offsets have been reported previously between the certified and measured element concentrations in different matrices (e.g., Gaboardi and Humayun, 2009). The divergence from the certified concentration is assigned to matrix effects, which may cause unequal fractionation of elements at the ablation site and in the plasma.

4. Results

Cathodoluminescence and trace element contents in quartz were studied in thin sections (300 µm thick) from 23 samples of granites, greisens and quartz representing the 1600 m long vertical section through the Cínovec granite pluton and associated Sn-W-Li deposit along borehole CS-1. Additional samples represent the greisen bodies and quartz–zinnwaldite veins within the deposit.

4.1. Shapes of quartz grains and crystals

Several basic types of quartz crystals (grains) were defined based on their shapes in classical optical microscope; their internal fabrics were visualized using SEM-CL images (Fig. 3).

Magmatic quartz in both biotite and zinnwaldite granite usually forms isometric, often rounded grains, traditionally termed as "drop-like" quartz, 1–5 m across, with regular low-intensity internal CL zoning (Fig. 3a). In the upper part of the zinnwaldite granite intrusion, quartz grains often contain numerous tiny inclusions of albite oriented along growth zones in quartz ("snow-ball" texture). A porphyritic variety of the biotite granite, the biotite microgranite, sometimes contains aggregates of several quartz grains with more intensive internal CL zoning (Fig. 3b).

Table 1
List of samples.

No.	Localization	Rock type
5459	Old dump in the southern part of the deposit	Explosive breccia with rhyolite clasts cemented by zinnwaldite microgranite
5462	Borehole CiW-11, depth 156.7 m	Rhyolite breccia cemented by zinnwaldite microgranite
4683	Borehole CS-1, depth 97 m	Medium grained zinnwaldite granite
4972	CS-1, 149 m	Quartz-rich greisen with cavities (5 mm across) with small crystals of quartz and zinnwaldite
4930	CS-1, 154 m	Compact quartz-zinnwaldite greisen
4931	CS-1, 155 m	Porous zinnwaldite-quartz greisen with fluorite
4973	CS-1, 163 m	Quartz-rich greisen with cavities (5 mm across) with small crystals of zinnwaldite and clay
4685	CS-1, 206 m	Medium grained zinnwaldite granite with hydrothermal alteration
4933	CS-1, 308 m	Medium-grained mica-free granite rich in feldspars
4686	CS-1, 337 m	Medium-grained mica-free granite rich in feldspars
4687	CS-1, 414 m	Porphyritic zinnwaldite granite with very fine groundmass, “zinnwaldite microgranite”
4688	CS-1, 560 m	Medium grained zinnwaldite granite
4689	CS-1, 735 m	Medium grained zinnwaldite granite
4690	CS-1, 741 m	Porphyritic biotite granite with very fine groundmass, “biotite microgranite”
4801	CS-1, 774 m	Medium grained biotite granite
4802	CS-1, 860 m	Porphyritic biotite granite with very fine groundmass, “biotite microgranite”
4941	CS-1, 1245 m	Porphyritic biotite granite with very fine groundmass, “biotite microgranite”
4942	CS-1, 1400 m	Medium grained biotite granite
4693	CS-1, 1580 m	Medium grained biotite granite
5412	Bünaustollen, old mining directly at the Czech-German border	Large steep body of quartz-rich greisen with wolframite
4980	Former “Main shaft” of Cínovec, upper horizon of the old mining	Quartz-zinnwaldite vein with wolframite and cassiterite
4982	Former “Main shaft” of Cínovec, upper horizon of the old mining	Quartz-zinnwaldite vein with wolframite and cassiterite
4983	Former “Main shaft” of Cínovec, upper horizon of the old mining	Quartz-zinnwaldite vein with wolframite and cassiterite

In greisen, quartz contents usually exceed the contents of all other minerals (mica, topaz, fluorite, ore minerals) together. Remnants of primary magmatic quartz show irregularly shaped CL-active cores surrounded by CL-free zone of newly formed quartz or quartz which equilibrated with the greisenizing fluid. Greisen-stage quartz grains replacing primary feldspars are generally xenomorphic and free of CL (Fig. 3c). Greisen contains occasional cm-sized cavities surrounded by quartz and mica crystals up to 5 mm long. These crystals are often euhedral and have intensive CL zoning. The youngest milky quartz forms thin coatings on the surface of some cavities (Fig. 3d).

Up to 20 cm long, perfectly bounded crystals of smoky and colorless quartz are known from vugs in quartz–zinnwaldite veins from old mine workings (hereafter termed as “crystals”). Colorless quartz is strongly oscillatory zoned in CL (Fig. 3e), while the smoky quartz (Fig. 3f) shows only irregular sector zoning. Some of these crystals are also coated with a tiny (mm) layer of milky quartz, which often developed only on some crystals faces. Milky quartz is conspicuous in the microscope, showing high concentration of fluid inclusions.

4.2. Chemical composition of quartz

The primary database contains approximately 650 spot analyses, 15–50 analyses from each of the 23 samples. Data from individual spots, after elimination of less than 5% of incidental errors (e.g., hits of mineral inclusions), are presented in Supplementary Table 1; data presented in Table 2 represent median values of the samples.

The contents of **Ti** (Fig. 4a) range from < 0.6 ppm to about 130 ppm. The contents decrease from BtG (10–130 ppm Ti) across ZiG (mostly 3–17 ppm) to greisen (< 1 ppm Ti in newly formed hydrothermal quartz, up to 15 ppm in relicts of magmatic quartz). In quartz crystals, colorless crystals are Ti-poor (< 5 ppm), while smoky quartz is slightly Ti-enriched (2–22 ppm Ti). The late milky quartz is poor in Ti (< 1 ppm).

Concentrations of **Ge**, a rare element chemically similar to silica, usually increase during fractionation, i.e., Ge increases slightly from ca. 0.5–1.5 ppm in BtG to 1–2.5 ppm in ZiG. Germanium contents in quartz from greisens and in quartz crystals from veins scattered mostly between 0.5–2.5 and 0.5–1.5 ppm, respectively (Fig. 4a).

Titanium is a compatible element in a granitic melt due to its ability to enter crystal lattice of early crystallizing mafic minerals, while Ge behaves as incompatible element concentrated in the residual melt. Thus, the Ge/Ti value in quartz was proposed as a reliable indicator of differentiation of magma from which the quartz crystallized (Jacamon and Larsen, 2009). This ratio is therefore used as a basis for visualizing the behavior of other analyzed elements during the evolution of the granite/greisens/veins system (Fig. 4b, d–h). In the studied samples, the Ge/Ti values ranged from ca. 0.01 to ca. 0.5 in individual analyses of magmatic quartz, and from ca. 0.05 to > 5 in hydrothermal quartz. Medians of samples are scattered between 0.02 and 0.28 in magmatic quartz, between 0.52 and 2.62 in quartz from greisens, and between 0.06 and 2.93 in quartz crystals from veins. The binary plot of Ge versus Ti (Fig. 4a) shows several entirely distinct trends: a strong decrease in Ti followed by an increase in Ge in the BtG, a wide scatter of Ge in all varieties of ZiG, low contents of Ti combined with a wide scatter of Ge in greisens and colorless crystals, and a positive Ge–Ti correlation in crystals of smoky quartz.

The contents of **Al** fluctuate between 8 ppm and 2279 ppm: Al contents in the ZiG (usually 100–400 ppm) are generally slightly higher than in the BtG (usually 80–250 ppm). Aluminium contents in greisens and crystals are comparatively low: 10–130 ppm and 8–100 ppm, respectively. Exceptional contents of 1395–2279 ppm were found in thin coatings of late milky quartz in small cavities in greisens and veins. There is a slight positive correlation between Al and the Ge/Ti value in magmatic quartz, no correlation in quartz from greisens, and a negative correlation in crystals of smoky quartz (Fig. 4b)

Lithium is, after Ti and Al, the third and the last element entering the crystal lattice of igneous quartz in larger amounts: mostly in the range of 10–50 ppm Li in both ZiG and BtG. The contents of Li in hydrothermal quartz from greisens and crystals is somewhat lower – mostly < 20 ppm. Only the late milky quartz is enriched, containing up to 99 ppm Li. Lithium is generally positively correlated with Al (Fig. 4c) but there is no correlation between Li and the Ge/Ti value (Fig. 4d).

Rubidium showed a wide variation: the highest contents up to 21 ppm were found in late milky quartz and quartz from the ZiG. Contents of about 5 ppm were found in quartz from the BtG and contents of < 1 ppm in quartz from greisens and crystals from veins (Fig. 4e). The contents of **Sr** are usually < 0.1 ppm with some exceptions of max. 0.8 ppm in greisens and maximum 2.8 ppm in milky quartz. The contents of **B** scattered mostly between 0.2 and 2 ppm, occasionally reaching up to 6 ppm in quartz from ZiG (Fig. 3f), while the contents of **Be** are slightly higher in granites (0.2–2.0 ppm) than in greisens (< 0.5 ppm) and crystals (< 0.2 ppm) (Fig. 4 g). The contents

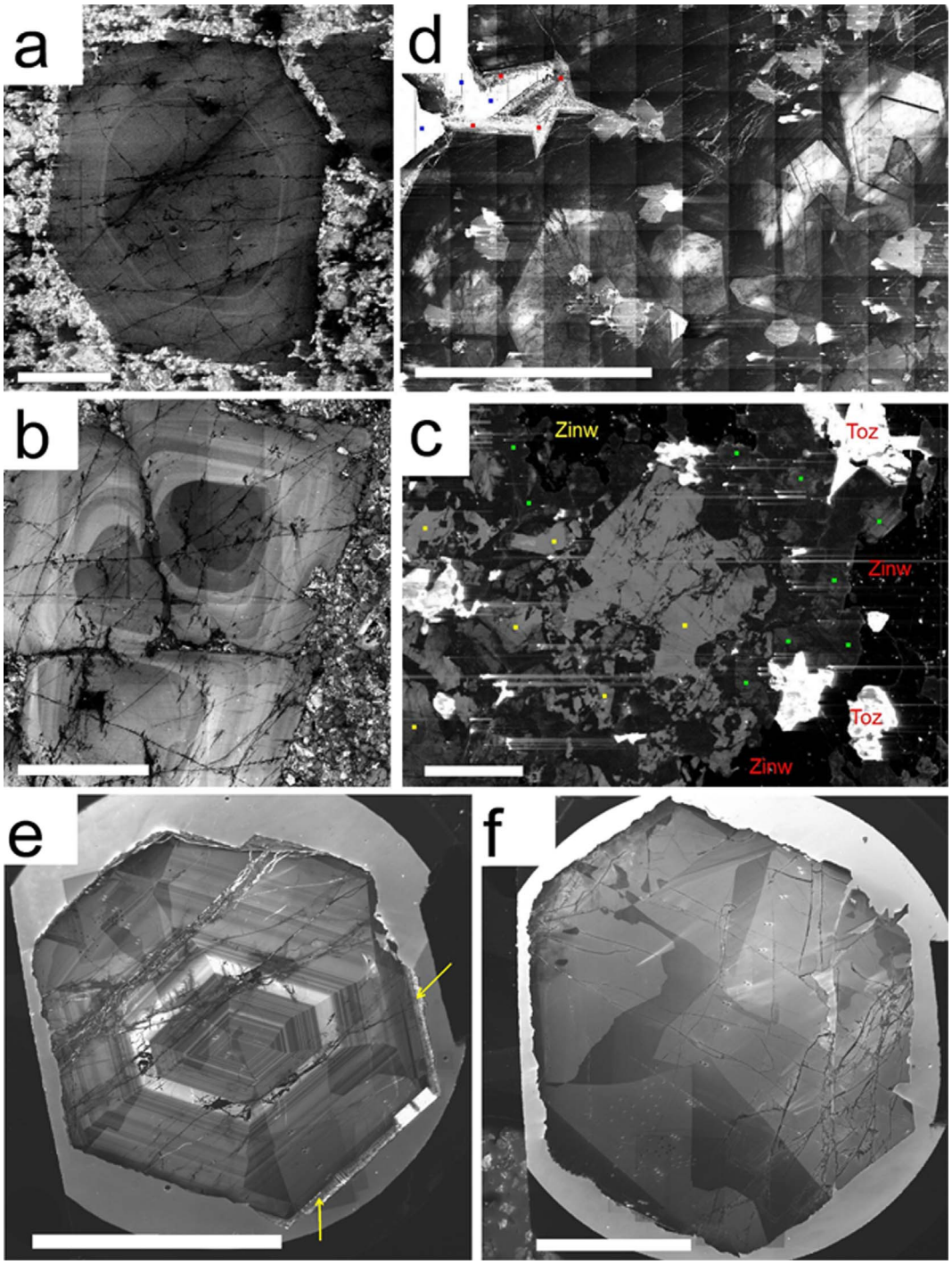

Fig. 3. Internal texture of quartz grains visualized by SEM-CL: a, regular zoning of quartz crystal indicates magmatic crystallization under stable conditions, #4687, zinnwaldite microgranite, depth of 413 m; b, assemblage of three quartz crystals with two-stage evolution: darker rounded cores are rimmed by oscillatory zoned rims, #4690 biotite microgranite, depth of 741 m; c, remnants of primary magmatic quartz with medium-intensive CL (highlighted by yellow points) surrounded and cemented by hydrothermal quartz with very weak CL (highlighted by green points). The bright grains with intensive CL are topaz, the black areas are zinnwaldite flakes. #4931 greisen with hydrothermal quartz replacing feldspars, depth of 155 m; d, quartz crystals with distinct CL-zoning are limited with crystal faces into small vugs. The open space of the vugs is highlighted by blue; the late generation of milky quartz covering the crystal faces is highlighted by red. Coarse-grained quartz-rich greisen with vugs, depth of 163 m, sample 4973; e, a colorless quartz crystal 3 cm long, 1.5 cm in diameter, thin coating of milky quartz is highlighted with yellow arrows, a cavity in a flat quartz vein, sample 4980; f, a crystal of smoky quartz, 4 cm long, 2.5 cm in diameter, a cavity in a flat quartz vein, sample 4982. Scale bars are 1 mm long in figs. a, b, c and 10 mm long in figs. d, e, f. (For interpretation of the references to colour in this figure legend, the reader is referred to the web version of this article.)

of **P** varied mostly within the interval of 2–10 ppm. Higher contents of max. 16 ppm were found in the ZiG cementing early magmatic breccia and max. 62 ppm in the late milky quartz. The contents of **Fe** are scattered usually between < 0.1 and 4 ppm in magmatic quartz, and between < 0.1 and 1 ppm in hydrothermal quartz; however, individual spots were found with up to 10 ppm Fe (Fig. 4h). The high contents of Fe do not correlate with Al and Li, which makes the contamination with inclusions of mica or other aluminosilicate unlikely. The contents of Mn are usually < 0.3 ppm. Higher values in the range of 0.4–4.5 ppm Mn were found in the lower part of the ZiG (depth of 560–735 m) and in the

Table 2
Medians of contents of trace elements in quartz in ppm (na- not analyzed).

No. of sample Det.limit	n	Li 0.2	Be 0.1	B 0.5	Ge 0.2	Al 5	P 5	Ti 0.6	Fe 0.5	Mn 0.2	Rb 0.03	Sr 0.04	Sn 0.1	Al/Ti	Ge/Ti
5459	31	22.9	0.36	1.5	1.37	244	13.9	7.65	2	< 0.2	< 0.03	< 0.04	0.16	32	0.18
5462	31	13.5	0.4	1.2	1.42	280	11.8	7.05	< 0.5	< 0.2	< 0.03	< 0.04	< 0.1	40	0.20
4683	11	14.8	0.76	2.2	1.53	258	8.5	7.1	na	0.5	0.40	0.1	na	36	0.22
4972	43	4.6	0.1	0.5	0.95	41	2.8	0.41	< 0.5	< 0.2	0.08	0.05	< 0.1	100	2.32
4930	47	1.7	0.23	0.7	1.1	45	4.1	0.42	< 0.5	< 0.2	0.13	0.09	< 0.1	107	2.62
4931	35	3.4	0.18	0.6	1.45	59	6.7	0.95	< 0.5	< 0.2	0.20	0.15	< 0.1	62	1.53
4973	57	1.9	0.08	< 0.5	1.14	43	2.9	0.82	< 0.5	< 0.2	0.04	0.06	< 0.1	52	1.39
4685	18	24.6	0.44	0.6	1.66	252	7.8	6.4	1.7	0.2	0.60	< 0.04	< 0.1	39	0.26
4933	40	27.5	0.82	1.0	1.71	245	< 5.0	9.2	1.3	0.2	3.60	0.05	< 0.1	27	0.19
4686	8	36.0	1.16	1.8	1.98	250	8.1	7.4	0.7	0.2	5.00	< 0.04	0.14	34	0.27
4687	47	16.5	0.57	1.0	1.09	192	6.2	14.2	2.1	0.3	0.70	0.07	< 0.1	14	0.08
4688	18	29.8	1.19	1.1	1.85	292	9.4	6.5	2.5	0.6	11.00	< 0.04	0.37	45	0.28
4689	20	24.8	1.17	1.1	1.7	249	10	6.83	2.3	0.4	8.50	< 0.04	0.18	36	0.25
4690	32	20.5	0.28	0.7	1.04	136	8.2	21.2	1.8	0.2	0.20	< 0.04	< 0.1	6	0.05
4801	10	27.0	0.8	0.7	1.4	176	< 5.0	16.4	2.3	< 0.2	0.60	0.08	< 0.1	11	0.09
4802	18	31.0	0.25	0.5	1.26	176	6.42	30.5	2.2	0.2	0.45	< 0.04	< 0.1	6	0.04
4941	12	23.2	0.27	< 0.5	0.82	147	6.9	54	1.5	< 0.2	0.15	0.2	< 0.1	3	0.02
4942	21	23.0	0.25	0.9	0.84	151	8.5	40	1.3	< 0.2	< 0.03	< 0.04	< 0.1	4	0.02
4693	16	17.0	1.17	2.4	0.98	148	8.15	22.3	na	0.8	0.20	< 0.04	< 0.1	7	0.04
5412	26	1.1	0.18	0.7	1.01	75	< 5.0	1.95	< 0.5	0.08	0.10	0.1	< 0.1	38	0.52
4980	19	10.7	0.10	< 0.5	0.84	48	< 5.0	< 0.6	< 0.5	< 0.2	< 0.03	0.05	< 0.1	92	1.62
4980 milky quartz	7	94	0.10	< 0.5	0.88	1395	8	< 0.6	2.3	3	18.00	1.1	< 0.1	4650	2.93
4982	16	6.8	< 0.10	1.8	0.84	26	6	14	< 0.5	< 0.2	< 0.03	0.04	< 0.1	2	0.06
4983	14	13	0.12	0.4	1.56	58	< 5.0	1.65	8.6	< 0.2	< 0.03	0.07	< 0.1	35	0.95

deepest sample of the BtG (depth 1580 m). Finally, the contents of **Sn** reached 0.1–0.2 (max. 0.6) ppm in granites but only < 0.1 ppm in greisens, crystals and late milky quartz.

4.3. Vertical zoning of magmatic quartz

The Cínovec granite cupola is, owing to the existence of the deep borehole CS-1, the first pluton where chemical composition of quartz can be studied along a vertical section over 1.5 km long (Fig. 5). Lithologies reached by the borehole are well reflected by Al contents (Fig. 5a): Al contents steadily increase upwards from the biotite granite (medians in the interval 136–176 ppm), across the older variety of zinnwaldite granite (microgranite at the depth of ca. 400 m, median 192 ppm), to the main variety of zinnwaldite granite including matrix of explosive breccia (medians 244–292 ppm). Predominantly hydrothermal quartz in greisen bodies shows strikingly low Al contents (medians 41–49 ppm). Vertical distribution of Ge (Fig. 5b) mimics this of Al but the trend is less conspicuous due to the ca. 100 times lower Ge contents. Titanium shows an opposite trend than Al, decreasing systematically upwards (Fig. 5a), while Li, B, and Be are scattered, showing no clear trend. Worth mentioning are the low Li contents in the uppermost 200 m interval (Fig. 5a). In breccia, the deficiency in Li can be attributed to Li escape with fluids after opening of the crystallizing system, while quartz in zinnwaldite granite and greisen crystallized mostly after Li-mica from a melt already impoverished in Li (compare Li-poor quartz from lepidolite pegmatites, Breiter et al., 2014).

The Al/Ti and Ge/Ti values illustrate the higher degree of ZiG fractionations, increasing noticeably upwards from BtG to ZiG over more than one order of magnitude, both values reaching their maxima in greisen bodies due to extremely low Ti contents in this type of quartz (Fig. 5c).

4.4. Chemical differences between magmatic and hydrothermal quartz

Four types of quartz with genetic connotation can be distinguished at Cínovec based on their chemical composition and textural and CL-properties:

- Primary magmatic quartz appears in both ZiG and BtG, usually as fine- to medium-grained groundmass quartz. In the porphyritic facies, it also appears in the form of phenocrysts. Its chemical composition is similar to that described from many other fractionated plutons (Müller et al., 2010; Breiter et al., 2013): 100–400 ppm Al generally increasing during fractionation, and 5–120 ppm Ti with an opposite trend. Crystals (grains) of magmatic quartz show usually regular internal zoning in the CL. Li contents in magmatic quartz are mostly > 10 ppm.
- Early hydrothermal (greisen stage) quartz is poor in both Al and Ti (generally < 100 ppm and < 5 ppm, respectively) and low, featureless CL signal. Irregular areas in cores of some grains showing moderate CL intensity show slightly elevated Ti contents (ca. 5–18 ppm); we interpret these areas as remnants of primary magmatic quartz not fully equilibrated with greisenizing fluids (Fig. 6). Quartz from greisen is conspicuously poor in Li (usually < 10 ppm) even though it crystallized together with zinnwaldite, i.e. from Li, F-rich fluids.
- Euhedral crystals of colorless quartz in cavities of quartz–zinnwaldite veins are chemically similar to the quartz from greisen (< 100 ppm Al, < 5 ppm Ti). Smoky quartz from the same locations differs in slightly higher Ti contents (up to 20 ppm) and a remarkable positive Al–Ti correlation. All crystals from cavities are poor in Li much like the quartz from greisen, reaching max. 15 ppm Li.
- Late hydrothermal (milky) quartz forms thin coating on the surface of older quartz in vugs in greisen bodies and quartz veins. This variety of quartz strongly differs in high contents of Al (ca. 500–2200 ppm), Li (80–99 ppm), Rb, Sr, Fe and Mn, and very low Ti contents (< 1 ppm). Very high Al combined with low Ti contents have been typically reported from low-temperature hydrothermal processes (Götte et al., 2011), epithermal Cu, Au, Ag and base metal deposits (Rusk et al., 2008) and barren quartz veins cutting greisen bodies in the western Erzgebirge (Breiter et al., 2017a). According to Rusk et al. (2008), high Al contents in low-temperature quartz resulted from high solubility of Al in acid solutions (pH < 3.5) at temperatures of ≤200 °C.

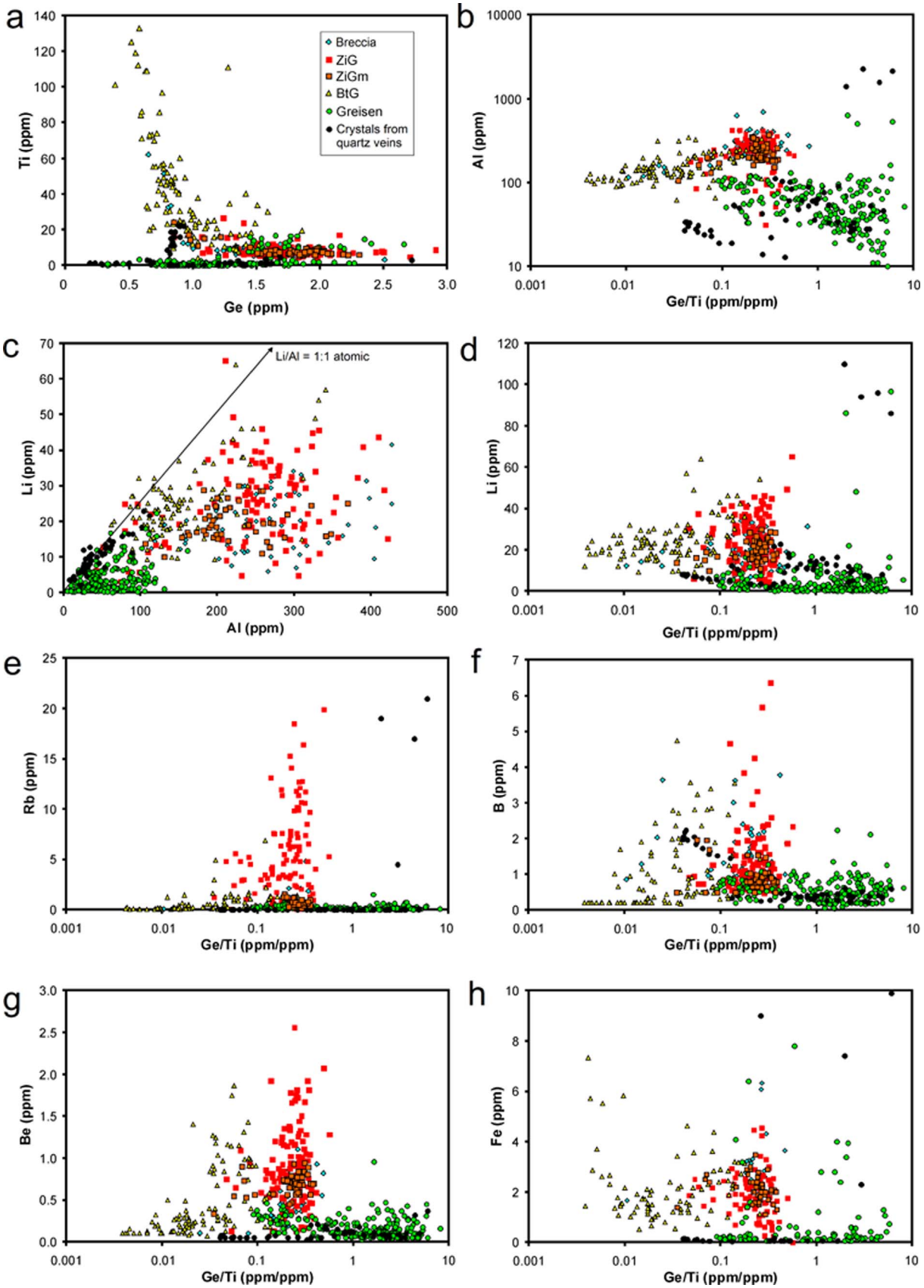

Fig. 4. Contents of trace elements in quartz: a, Ti *vs.* Ge; b, Al *vs.* Ge/Ti; c, Li *vs.* Al; d, Li *vs.* Ge/Ti; e, Rb *vs.* Ge/Ti; f, B *vs.* Ge/Ti; g, Be *vs.* Ge/Ti; h, Fe *vs.* Ge/Ti.

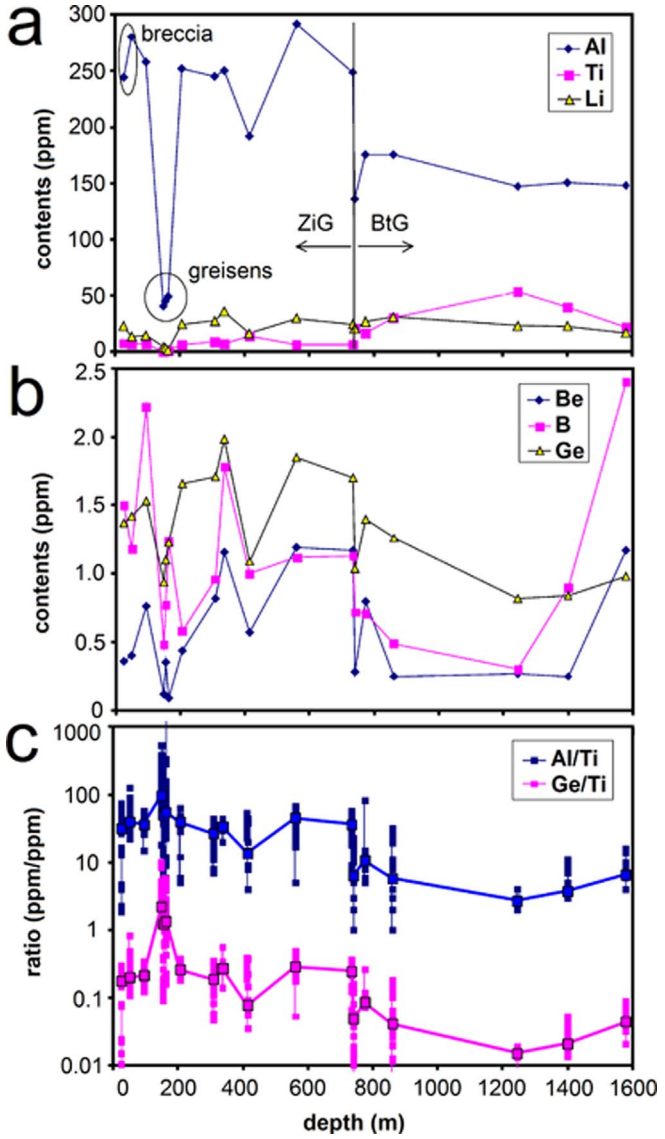

Fig. 5. Distribution of trace elements in quartz along the borehole CS-1 (in ppm): a, Al, Ti, Li; b, Be, B, Ge; c, Al/Ti, Ge/Ti. Two samples of the breccia, collected outside this borehole, are shown at the top of the profile for comparison. Only medians are shown in Figs. a, b, while all measurements with highlighted means are drown in Fig. c.

5. Discussion

5.1. Chemical zoning of quartz grains, thermobarometric considerations

In the studied granites, quartz grains with highly varied internal fabrics were found. The style of zoning is independent of the parent rock (Fig. 7):

1. grains with "normal" zoning, e.g., a decrease in Ti coupled with an increase in Al from core to rim like phenocryst #4942 from the BtG (Fig. 7b). More often, an outward decrease in Ti is combined with generally constant or irregularly scattered contents of Al, as in samples #5462 and #4933A in the ZiG (Fig. 7a), and in smoky quartz (#4982, Fig. 7d). In the case of greisen #4930 (Fig. 7c), the Ti-enriched domain represents an old magmatic core, rimmed by low-Ti zone of greisen-stage alteration and overgrowth.
2. grains with "inverse" zoning, e.g. with Ti increase from core to rim, have been reported from the Teplice rhyolite (Müller et al., 2005; Breiter et al., 2012) and were also found in the studied biotite granite (#4802, Fig. 7b).
3. grains with no distinct zoning are common, mainly in the ZiG (#4933B, #4687, Fig. 7a and b).
4. coatings of milky quartz are conspicuously enriched in Al (#4973 from greisen, Fig. 7c, and #4980 from a vein, Fig. 7d).

Internal chemical zoning of euhedral quartz crystals from rhyolites were used for thermometric interpretations of magma evolution (Müller et al., 2005, 2008b; Breiter et al., 2012). In the studied granites, quartz crystals with similar shapes but contrasting zoning co-exist within a single thin section. Different styles of zoning may indicate different ages of individual quartz grains, i.e., crystallization in different stages of the fractionation–ascent–admixture of residual melt–final crystallization processes. This made any interpretation of time-dependent evolution of the conditions of crystallization very speculative. Very roughly, using the pressure estimation by Müller et al. (2005), the curve of water-saturated granite minima by Johannes and Holtz (1996) and Ti-in quartz thermometer by Huang and Audétat (2012), the temperature of crystallization was near 650 °C for the biotite granite, and slightly lower for the zinnwaldite granite.

5.2. Comparison Ge/Ti vs. Al/Ti, influence of peraluminity on Al contents in magmatic quartz

During the last decade, most authors used the Al/Ti value in quartz as a reliable indicator of the evolution of magma from which the quartz crystallized (Müller et al., 2005, 2008a,b, 2010; Breiter and Müller, 2009; Beurlen et al., 2011; Breiter et al., 2012, 2013, 2014).

Nevertheless, Jacamon and Larsen (2009) questioned the credibility of this value and recommended to use the Ge/Ti value. The Al/Ti value may be, according to Jacamon and Larsen (2009), influenced by the peraluminity of parental granitic melt. Already in 2009, Breiter and Müller (2009) showed that high Al contents in late populations of quartz in rare metal granites are independent of the melt peraluminity. Recently, Garate-Olave et al. (2017) excluded any relationship between the peraluminity of melt and Al contents in quartz in the granite-pegmatite system at Tres Arroyos, Spain. Neither the presently studied samples from Cínovec revealed any correlation between Al in quartz and peraluminity expressed as ASI [aluminium saturation index = molar $Al_2O_3/(CaO + Na_2O + K_2O)$, Fig. 8a]. The ability of quartz to incorporate high amount of Al into its crystal lattice is supported mainly by the high content of water and Li as a charge-balancing element ($Si^{4+} \leftrightarrow Al^{3+} + Li^{+}$) in the melt. The Ge *vs.* Al plot (Fig. 8b) shows a relatively wide dispersion (poor correlation) between the two elements in magmatic quartz and even no correlation in greisen quartz. But, surprisingly, the Al/Ti and Ge/Ti values are well correlated (Fig. 8c): the magmatic and hydrothermal populations of quartz form two evolutionary trends, the hydrothermal being relatively enriched in Ge. We therefore conclude that both Ge/Ti and Al/Ti values can be used as indicators of magma fractionation giving very similar results.

5.3. Distinction of magmatic vs. hydrothermal quartz

Quartz aggregates in greisen (Fig. 3c) actually combine three genetic varieties of quartz: (i) intact magmatic quartz with no alteration preserving the primary contents of trace elements and primary intensity of CL; (ii) magmatic quartz altered *via* fluid infiltration and/or dissolution–reprecipitation processes; both these processes have a purifying effect, i.e., they diminish the contents of trace elements and thus the intensity of CL (Larsen et al., 2009); (iii) newly formed quartz crystallized from high-temperature hydrothermal fluids with low contents of trace elements and negligible CL. Quartz domains altered to a variable degree (type ii quartz) may form a continual transition between magmatic (type i) and hydrothermal (type iii) quartz, and setting the exact boundary between quartz of different origin is not possible. The presence of altered (type ii) quartz is also the most probable source of the wide dispersion in the contents of Al, Li, Ge, and Fe in quartz

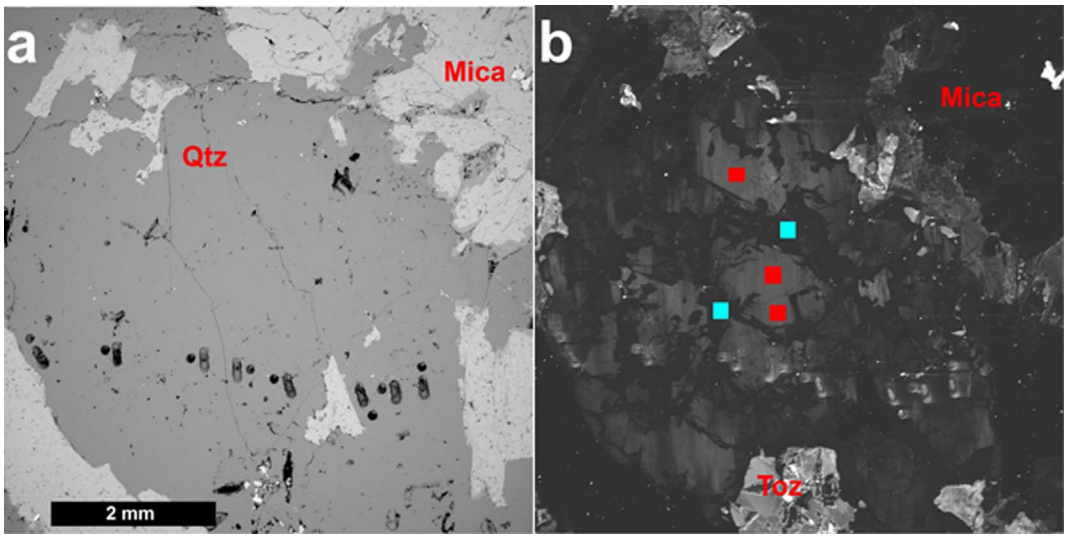

Fig. 6. Texture of quartz from a quartz-zinnwaldite greisen (#4931) visualized in BSE (a) and CL (b): Quartz grains are homogeneous in BSE image, while in the CL image, the CL-active (bright) remnants of magmatic quartz and CL-inactive (dark) in greisen-stage re-equilibrate and/or newly formed quartz are well distinguishable. Red marks- 10–11 ppm Ti, blue marks- 1–2 ppm Ti. Associated topaz (Toz) is bright in CL, while mica (zinnwaldite) is CL-inactive. (For interpretation of the references to colour in this figure legend, the reader is referred to the web version of this article.)

from greisen samples (Fig. 4).

5.4. Comparison with quartz from other geological environments

In Fig. 9, chemical evolution of quartz from Cínovec is compared with the evolution of quartz from pegmatites and granitoid plutons of different geochemical/geotectonic affiliations. This comparison employed well documented magmatic systems from the Bohemian Massif (Breiter and Müller, 2009; Breiter et al., 2012, 2013, 2014). This figure documents an intensive fractionation of the Teplice rhyolite melt, the immediate magmatic forerunner of the Cínovec granite within the Altenberg–Teplice caldera: the degree of rhyolite fractionation expressed by the Al/Ti and Ge/Ti values in quartz, parallels with the fractionation from the BtG to ZiG at Cínovec. The evolution of A-type

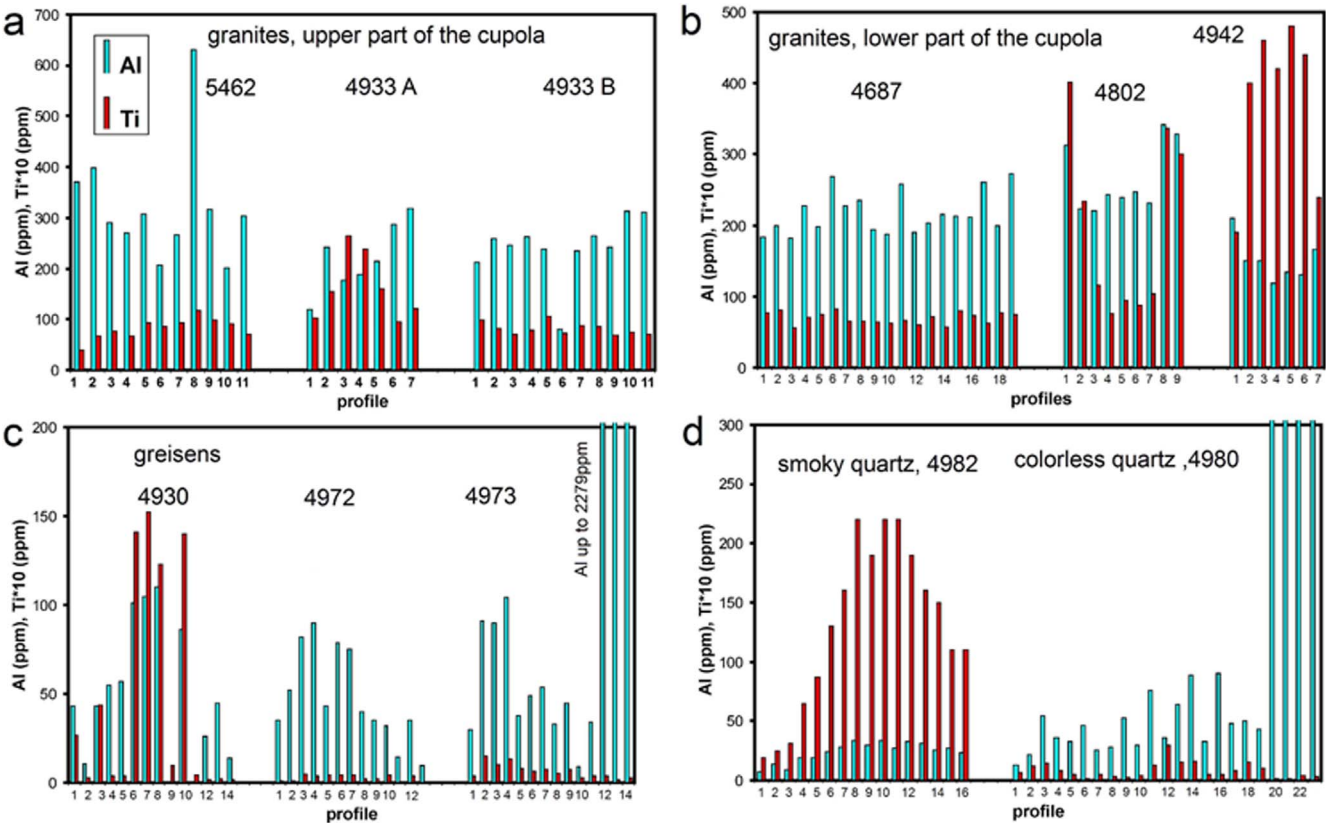

Fig. 7. Contents of Al and Ti across different types of quartz crystals/aggregates: a, quartz in the upper part of the zinnwaldite granite intrusion; b, quartz from the deeper part of the zinnwaldite granite (#4687), biotite granite (#4802) and biotite microgranite (#4942); c, quartz from greisen; d, quartz crystals from cavities in quartz-zinnwaldite veins. For localization of samples see Table 1.

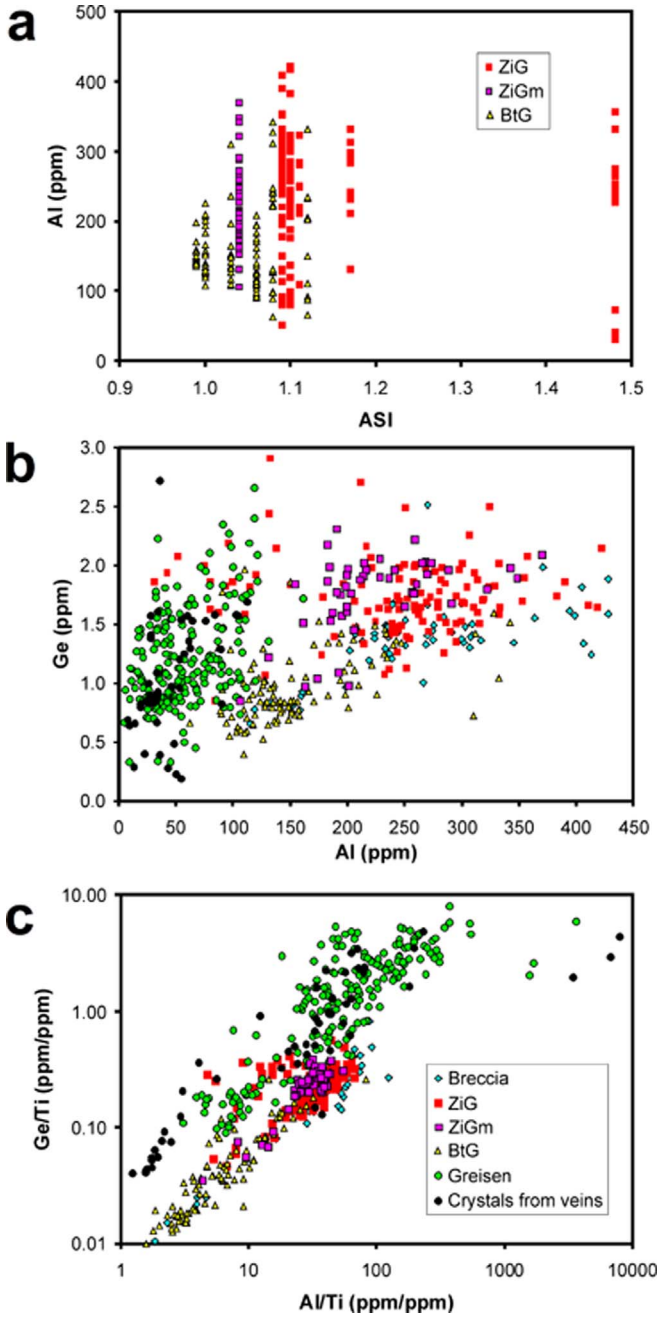

Fig. 8. The behavior of Al and Ge during fractionation: a, Al *vs.* ASI; b, Ge *vs.* Al; c, Ge/Ti *vs.* Al/Ti.

granites from the Hora Svaté Kateřiny pluton in the Central Erzgebirge is fully comparable with Cínovec.

This figure also shows a significant relative Al enrichment in quartz from the peraluminous Nejdek pluton, Western Erzgebirge, while all pegmatites are relatively enriched in Ge; relative enrichment in Ge has been proposed as a typical feature of pegmatites already by Schrön et al. (1988). In this context, the enrichment in Ge found in quartz from granites from the Rozvadov pluton (at the Czech/Bavarian border) is in agreement with the strong pegmatite fertility of this pluton (Breiter and Siebel, 1995). The Al/Ti and Ge/Ti values in less evolved two-mica granites from the Moldanubicum (southern Czech Republic/Austria) are significantly lower than in the above mentioned rare-metal granites. The lowest Al/Ti values, albeit with some relative Ge enrichment, were found in quartz from the calc-alkaline (I-type) Central Bohemian pluton.

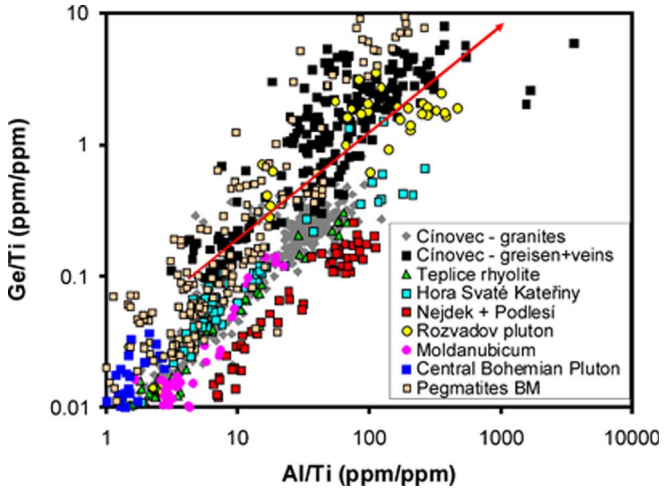

Fig. 9. A comparison of quartz from Cínovec with quartz from different silica-rich magmatic systems: Teplice A-type rhyolite (data from Breiter et al., 2012), Hora Svaté Kateřiny A-type rare-metal granite (data from Breiter and Müller, 2009), S-type rare-metal granites from the Nejdek and Rozvadov plutons, S-type two-mica granites from the Moldanubicum and I-type from the Central Bohemian pluton (all data from Breiter et al., 2013). Quartz data from different types of pegmatites from the Bohemian Massif (Breiter et al., 2014) and the evolutionary trend of the Tres Arroyos granite pegmatite system from Spain (red arrow, Garate-Olave et al., 2017) are also shown.

Recent data from the Tres Arroyos peraluminous granite-pegmatite system in Spain (Garate-Olave et al., 2017) showed a relative Ge enrichment in quartz from the whole magmatic suite and confirmed the above mentioned ability of pegmatite quartz to concentrate Ge relative to Al and Ti.

6. Conclusions

Some of the measured trace elements in quartz provide reliable information for genetic considerations, especially the contents of Al, Ti and Li, and the Al/Ti and Ge/Ti values. Individual spot analyses scattered, but the medians of individual samples sufficiently characterized evolutionary trends and particular properties of different rock types.

Pronounced fractionation from biotite granite to zinnwaldite granite is highlighted by an increase in Al (from 136–176 to 240–280 ppm) and Ge (from 0.8–1.2 to 1.1–1.7 ppm), and a decrease in Ti (from 16–54 to 6–14 ppm), which is expressed in a strong increase in the Al/Ti and Ge/Ti values (from 3–11 to 14–45 and from 0.02–0.09 to 0.08–0.28, respectively).

In greisen, newly formed metasomatic quartz is distinguishable from the remnants of magmatic quartz, the latter having more intensive CL and higher Ti content (> 10 ppm). Hydrothermal quartz from greisens and veins is poor in all trace elements, containing typically < 60 ppm Al, < 10 ppm Li, and < 1 ppm Ti. Nevertheless, a part of primary magmatic quartz may by secondarily purified *via* infiltration of hydrothermal fluids and/or dissolution–reprecipitation processes. Then, its chemical and CL properties become identical with those of newly formed greisen-stage quartz. Therefore, the share of greisen-stage quartz may by overestimated.

The youngest milky quartz, forming thin coatings on older hydrothermal quartz, is strongly enriched in Al (> 1000 ppm) and Li (~100 ppm), which indicates a more acid reaction of the late low-temperature fluids.

Internal zoning of magmatic quartz crystals visualized by CL proved a common occurrence of different zoning patterns, which may indicate different ages of crystallization of individual quartz grains during the emplacement and crystallization of volatile-rich magma.

Acknowledgements

This work was supported by Research Plan RVO 67985831 of the Institute of Geology of the Czech Academy of Sciences. Detailed, critical but inspiring and helpful reviews by R.B. Larsen (Tromsø) and A.B. Müller (Oslo) helped us to improve the manuscript significantly.

Appendix A. Supplementary data

Supplementary data associated with this article can be found, in the online version, at http://dx.doi.org/10.1016/j.oregeorev.2017.10.013.

References

Beurlen, H., Müller, A., Silva, D., Silva, M.R.R.D., 2011. Petrogenetic significance of LA-ICP-MS trace-element data on quartz from the Borborema pegmatite province, northeast Brazil. Mineral. Mag. 75, 2703–2719.

Breiter, K., 1997. Teplice rhyolite (Krušné hory Mts., Czech Republic): chemical evidence of a multiply exhausted stratified magma chamber. Bull. Czech Geol. Surv. 72, 205–213.

Breiter, K., Müller, A., 2009. Evolution of rare metal-specialised granite melt documented by quartz chemistry. Eur. J. Miner. 21, 335–346.

Breiter, K., Siebel, W., 1995. Granitoids in the Rozvadov Pluton, Western Bohemia and Oberpfalz. Evolution of the Variscan (Hercynian)and Comparable Orogenic Belts. Geol. Rundsch. 84, 506–519.

Breiter, K., Škoda, R., 2012. Vertical zonality of fractionated granite plutons reflected in zircon chemistry: the Cínovec A-type versus the Beauvoir S-type suite. Geol. Carpat. 63, 383–398.

Breiter, K., Škoda, R., 2017. Zircon and whole-rock Zr/Hf ratios as markers of the evolution of granitic magmas: examples from the Teplice caldera (Czech Republic/Germany). Mineral. Petrol. 111, 435–457.

Breiter, K., Förster, H., Seltmann, R., 1999. Variscan silicic magmatism and related tin-tungsten mineralization in the Erzgebirge-Slavkovský les metamollgenic province. Miner. Depos. 34, 505–521.

Breiter, K., Svojtka, M., Ackerman, L., Švecová, K., 2012. Trace element composition of quartz from the Variscan Teplice caldera (Krušné hory/Erzgebirge Mts., Czech Republic/Germany): Insights into the volcano-plutonic complex evolution. Chem. Geol. 326–327, 36–50.

Breiter, K., Ackerman, L., Svojtka, M., Müller, A., 2013. Behaviour of trace elements in quartz from plutons of different geochemical signature: a case study from the Bohemian Massif, Czech Republic. Lithos 175–176, 54–67.

Breiter, K., Ackerman, L., Ďurišová, J., Svojtka, M., Novák, M., 2014. Trace element composition of quartz from different types of pegmatites: a case study from the Moldanubian Zone of the Bohemian Massif (Czech Republic). Mineral. Mag. 78, 703–722.

Breiter, K., Ďurišová, J., Dosbaba, M., 2017a. Response of quartz chemistry to greisenization: Preliminary results from the western Krušné hory/Erzgebirge. Geosci. Res. Rep. 50, 25–31 (in Czech with English abstract).

Breiter, K., Ďurišová, J., Hrstka, T., Korbelová, Z., Hložková Vaňková, M., Vašinová Galiová, M., Kanický, V., Rambousek, P., Knésl, I., Dobeš, P., Dosbaba, M., 2017b. Assessment of magmatic *vs.* metasomatic processes in rare-metal granites: a case study of the Cínovec/Zinnwald Sn-W-Li deposit, Central Europe. Lithos 292–293, 198–217.

Cocherie, A., Johan, V., Rossi, Ph., Štemprok, M., 1991. Trace-element variation and lanthanide tetrad effect studied in a Variscan lithium granite: case of the Cínovec granite (Czechoslovakia). In: Pagel, M., Leroy, J.L. (Eds.), Source, transport and deposition of metals. Proceedings of SGA Anniversary Meeting, pp. 745–749.

D'Lemos, R.S., Kearsley, A.T., Pembroke, J.W., Watt, G.R., Wright, P., 1997. Komplex quartz growth histories in granite revealed by scanning cathodoluminescence techniques. Geol. Mag. 134 549–542.

Donovan, J.J., Lowers, H.A., Rusk, B.G., 2011. Improved electron probe microanalysis of trace elements in quartz. Am. Mineral. 96, 274–282.

Flem, B., Bédard, L.P., 2002. Determination of trace elements in BCS CRM 313/1 (BAS) and NIST SRM 1830 by inductively coupled plasma-mass spectrometry and instrumental neutron activation analysis. Geostand. Newslett. 26, 287–300.

Flem, B., Larsen, R.B., Grimstvedt, A., Mansfeld, J., 2002. In situ analysis of trace elements in quartz by using laser ablation inductively coupled plasma mass spectrometry. Chem. Geol. 182, 237–247.

Förster, H.-J., Trumbull, R.B., Gottesmann, B., 1999. Late-collisional granites in the Variscan Erzgebirge, Germany. J. Petrol. 40, 1613–1645.

Frelinger, S.N., Ledvina, M.D., Kyle, J.R., Zhao, D., 2015. Scanning electron microscopy cathodoluminescence of quartz: principles, techniques and application in ore geology. Ore Geol. Rev. 65, 840–852.

Gaboardi, M., Humayun, M., 2009. Elemental fractionation during LA-ICP-MS analysis of silicate glasses: implications for matrix-independent standardization. J. Anal. At. Spectrom. 24, 1188–1197.

Garate-Olave, I., Müller, A., Roda-Robles, E., Gil-Crespo, P.P., Pesquera, A., 2017. Extreme fractionation in a granite–pegmatite system documented by quartz chemistry: the case study of tres Arroyos (Central Iberian Zone, Spain). Lithos 286–287, 162–174.

Götte, T., Pettke, T., Ramseyer, K., Koch-Müller, M., Mullis, J., 2011. Cathodoluminescence properties and trace element signature of hydrothermal quartz: a fingerprint of growth dynamics. Am. Mineral. 96, 802–813.

Götze, J., Plötze, M., Graupner, T., Hallbauer, D.K., Bray, C.J., 2004. Trace element incorporation into quartz: a combined study by ICP-MS, electron spin resonance, cathodoluminescence, capillary ion analysis, and gas chromatography. Geochim. Cosmochim. Acta 68, 3741–3759.

Huang, R., Audétat, A., 2012. The titanium-in-quartz (TitaniQ) thermobarometer: a critical examination and re-calibration. Geochim. Cosmochim. Acta 84, 75–89.

Jacamon, F., Larsen, R.B., 2009. Trace element evolution of quartz in the charnockitic Kleivan granite, SW-Norway: the Ge/Ti ratio of quartz as an index of igneous differentiation. Lithos 107, 281–291.

Johan, V., Johan, Z., 1994. Accessory minerals of the Cínovec (Zinnwald) granite cupola, Czech Republic. Part 1: Nb-, Ta- and Ti-bearing oxides. Mineral. Petrol. 51, 323–343.

Johannes, W., Holtz, F., 1996. Petrogenesis and Experimental Petrology of Granitic Rocks. Springer, Berlin, Heidelberg, New York.

Larsen, R.B., Henderson, I., Ihlen, P.M., Jacamon, F., 2004. Distribution and petrogenetic behaviour of trace elements in granitic pegmatite quartz from South Norway. Contrib. Mineral. Petrol. 147, 615–628.

Larsen, R.B., Jacamon, F., Kronz, A., 2009. Trace element chemistry and textures of quartz during the magmatic hydrothermal transition of Oslo rift granites. Mineral. Mag. 73, 691–707.

Monecke, T., Kempe, U., Götze, J., 2002. Genetic significance of the trace element content in metamorphic and hydrothermal quartz: a reconnaissance study. Earth Planet. Sci. Lett. 202, 709–724.

Müller, A., Koch-Müller, M., 2009. Hydrogen speciation and trace element contents of igneous, hydrothermal and metamorphic quartz from Norway. Mineral. Mag. 73, 569–583.

Müller, A., Seltmann, R., Behr, H.J., 2000. Application of cathodoluminescence to magmatic quartz in a tin granite – case study from the Schellerhau Granite Complex, Eastern Erzgebirge, Germany. Miner. Depos. 35, 169–189.

Müller, A., Wiedenbeck, M., van den Kerkhof, A.M., Kronz, A., Simon, K., 2003. Trace elements in quartz – a combined electron microprobe, secondary ion mass spectrometry, laser-ablation ICP-MS, and cathodoluminescence study. Eur. J. Mineral. 15, 747–763.

Müller, A., Breiter, K., Seltmann, R., Pécskay, Z., 2005. Quartz and feldspar zoning in the eastern Erzgebirge volcano-plutonic complex (Germany, Czech Republic): evidence of multiple magma mixing. Lithos 80, 201–227.

Müller, A., Ihlen, P.M., Kronz, A., 2008a. Quartz chemistry in polygeneration Sveconorwegian pegmatites, Froland, Norway. Eur. J. Mineral. 20, 447–463.

Müller, A., Seltmann, R., Kober, B., Eklund, O., Jeffries, T., Kronz, A., 2008b. Compositional zoning of Rapakivi feldspars and coexisting quartz phenocrysts. Can. Mineral. 46, 1417–1442.

Müller, A., van den Kerkhof, A.M., Behr, H.-J., Kronz, A., Koch-Müller, M., 2010. The evolution of late-Hercynian granites and rhyolites documented by quartz – a review. Earth Environ. Trans. R. Soc. Edinburg 100, 185–204.

Rub, A.K., Štemprok, M., Rub, M.G., 1998. Tantalum mineralization in the apical part of the Cínovec (Zinnwald) granite stock. Mineral. Petrol. 63, 199–222.

Rusk, B.G., Reed, M.H., Dilles, J.H., Kent, J.R., 2006. Intensity of quartz cathodoluminescence and trace-element content in quartz from the porphyry copper deposit at Butte, Montana. Am. Mineral. 91, 1300–1312.

Rusk, B.G., Lowers, H.A., Reed, M.H., 2008. Trace elements in hydrothermal quartz: relationship to cathodoluminescent textures and insights into vein formation. Geology 36, 547–550.

Schrön, W., Schmädicke, E., Thomas, R., Schmidt, W., 1988. Geochemische Untersuchungen an Pegmatitquarzen. Z. Geol. Wiss. 16, 229–244.

Seltmann, R., Wetzel, H.-U., Felix, M., Schilka, W., 1987. Brekzien der Altenberger Scholle. Exkursion Führer 34. Jahrestagung der Gessellschaft für geologische Wissenschaften DDR, Berlin.

Štemprok, M., Šulcek, Z., 1969. Geochemical profile through an ore-bearing lithium granite. Econ. Geol. 64, 392–404.

Takahashi, R., Müller, A., Matsueda, H., Okrugin, V.M., Shuji, O., van der Kerkhof, A., Kronz, A., Andreeva, E.D., 2007. Cathodoluminescence and trace elements in quartz: clues to metal precipitation mechanism at the Asachinskoe gold deposit in Kamchatka. In: Okada, H., Mawatari, S.F., Suzuki, N., Guatam, P. (eds.), Origin and evolution of natural diversity, Proceeding of international symposium "The origin and evolution of natural diversity" Sapporo, 175–184.

Walther, D., Breitkreuz, C., Rapprich, V., Kochergina, Y.V., Chlupáčová, M., Lapp, M., Magna, T., 2016. The late Carboniíferous Schönfeld-Altenberg depression on the NW margin of the Bohemian Massif (Germany/Czech Republic): volcanosedimentary and magmatic evolution. J. Geosci. 61, 371–393.